



# Semiconductor spintronics with Co<sub>2</sub>-Heusler compounds

Kohei Hamaya\*<sup>1</sup> and Michihiro Yamada

Ferromagnetic Co<sub>2</sub>-Heusler compounds showing high spin polarization have been utilized as spin injectors and detectors for III–V and Group-IV semiconductors. In this article, we first describe the progress in the crystal growth of Co<sub>2</sub>-Heusler films on GaAs(001) and Ge(111) by low-temperature molecular beam epitaxy. Next, some examples of electrical spin injection from Co<sub>2</sub>-Heusler contacts into GaAs and Ge through Schottky-tunnel barriers are introduced. Thanks to those efforts, it was found that Co<sub>2</sub>-Heusler compounds are useful for the realization of spin injection, transport, and detection in GaAs and Ge at room temperature. However, to achieve highly efficient spin transport, it is very important to suppress the interfacial out-diffusion of GaAs or Ge into the Co<sub>2</sub>-Heusler layer near the heterojunction. Recent progress in high-quality Co<sub>2</sub>-Heusler/Ge heterojunctions has demonstrated two-terminal magnetoresistance ratios of more than 0.1% at room temperature even for semiconductor spintronic device structures. The approach using Co<sub>2</sub>-Heusler compounds provides a powerful solution to the need for simultaneous achievement of highly efficient spin injection and low electric power at the source and drain contacts in semiconductor devices such as a spin MOSFET.

## Introduction

Ferromagnetic Co<sub>2</sub>-Heusler compounds with the chemical formula Co<sub>2</sub>YZ, where Y is a transition metal and Z is a main group element such as Si and Ge, are candidate materials for half-metals with a fully spin-polarized (100% spin polarization) density of states (DOS) at the Fermi level.<sup>1–3</sup> For spintronic memory and sensor applications,<sup>4,5</sup> a number of high-performance Co<sub>2</sub>-Heusler compounds have already been reported as ferromagnetic electrodes in magnetic tunnel junctions (MTJs),<sup>6–9</sup> current-perpendicular-to-plane giant magnetoresistive (CPP-GMR) devices,<sup>10–13</sup> and lateral spin-valve (LSV) devices.<sup>14–16</sup>

In the field of semiconductor spintronics,<sup>17–27</sup> the use of Co<sub>2</sub>YZ has been proposed for spin injector and detector contacts in spin-based light-emitting diodes (LEDs) and field-effect transistors (FETs).<sup>28–30</sup> **Figure 1a–b** shows schematics of a spin FET, proposed by Datta and Das,<sup>31</sup> and a spin metal–oxide–semiconductor (MOS) FET, proposed by Sugahara and Tanaka,<sup>32,33</sup> respectively. Here, the source/drain (S/D) contacts are composed of a ferromagnetic (FM) material and FM/semiconductor heterojunctions. Although the device

structures of both types of spin transistors are almost the same, quite different operating principles have been proposed, involving spin transport in III–V semiconductor channels with a large spin–orbit interaction<sup>31</sup> or in Group-IV semiconductor channels with a small spin–orbit interaction.<sup>32,33</sup> For the Datta and Das spin FET, because electrons' spins are controlled by an electric field via the Rashba spin–orbit coupling in the III–V semiconductor channels, it is not necessary to change the magnetization direction of the FM materials at the SD contacts.<sup>31</sup> For the Sugahara and Tanaka spin MOSFET, on the other hand, the output signal is related to the spin-dependent transport through the Group-IV semiconductor channels, depending on the magnetization direction of the FM materials at the SD contacts.<sup>32,33</sup> In particular, if one can realize a high-performance spin MOSFET on a Si platform, nonvolatile memory devices can be integrated into CMOS transistors.<sup>33,34</sup> To achieve highly efficient spin-dependent transport in these FETs, electrical spin injection, transport, and detection in III–V or Group-IV semiconductor channels with Co<sub>2</sub>YZ S/D contacts should be explored.

Kohei Hamaya, Center for Spintronics Research Network, Graduate School of Engineering Science, Osaka University, Toyonaka, Osaka, Japan; Department of Systems Innovation, Graduate School of Engineering Science, Osaka University, Toyonaka, Osaka, Japan; hamaya.kohei.es@osaka-u.ac.jp

Michihiro Yamada, Center for Spintronics Research Network, Graduate School of Engineering Science, Osaka University, Osaka, Japan; PRESTO, Japan Science and Technology Agency, Kawaguchi, Saitama, Japan; michihiro@ee.es.osaka-u.ac.jp

\*Corresponding author

doi:10.1557/s43577-022-00351-0

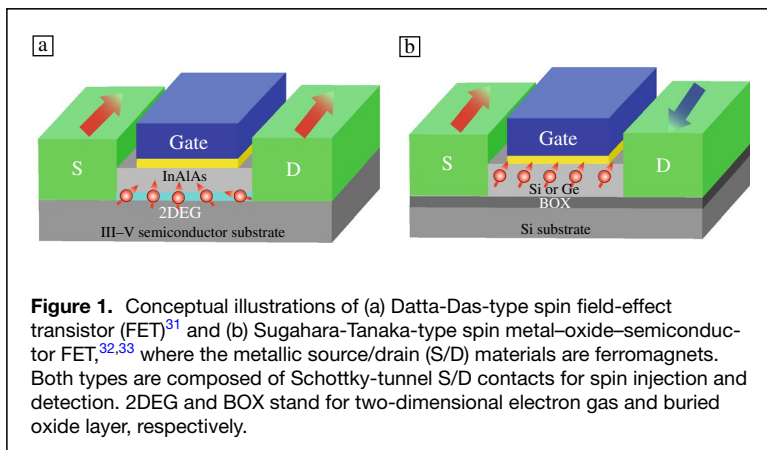


**Figure 1.** Conceptual illustrations of (a) Datta-Das-type spin field-effect transistor (FET)<sup>31</sup> and (b) Sugahara-Tanaka-type spin metal-oxide-semiconductor FET,<sup>32,33</sup> where the metallic source/drain (S/D) materials are ferromagnets. Both types are composed of Schottky-tunnel S/D contacts for spin injection and detection. 2DEG and BOX stand for two-dimensional electron gas and buried oxide layer, respectively.

One of the most important parameters for Co<sub>2</sub>YZ is the structural order. The top illustration in **Figure 2a–b** is the crystal structures of *L*<sub>21</sub>-ordered Co<sub>2</sub>YZ. When the Y-site atoms are randomly replaced by the Z-site atoms, it is a so-called *B*<sub>2</sub>-ordered structure. If Co, Y, and Z atoms occupy all the sites randomly, it is not an ordered structure but is an *A*<sub>2</sub> structure. In general, *B*<sub>2</sub>- or *L*<sub>21</sub>-ordered structures are required to obtain high-performance spintronic devices.<sup>2,3</sup> For MTJs and CPP-GMR devices, high-temperature annealing treatments (~550°C) are generally performed to promote the formation of *B*<sub>2</sub>- or *L*<sub>21</sub>-ordered structures.<sup>6–13</sup> However, because these high-temperature annealing treatments are not compatible with the formation of heterostructures consisting of Co<sub>2</sub>YZ and semiconductors, low-temperature formation techniques are required. Thus, crystal growth of Co<sub>2</sub>YZ films with *B*<sub>2</sub>- or *L*<sub>21</sub>-ordered structures on semiconductors has been explored. In particular, because the lattice parameters for Co<sub>2</sub>YZ compounds such as Co<sub>2</sub>MnSi and Co<sub>2</sub>FeSi are nearly equivalent to those for GaAs and Ge, low-temperature growth methods by molecular beam epitaxy (MBE) are attractive for achieving *B*<sub>2</sub>- or *L*<sub>21</sub>-ordered structures without

forming magnetic dead layers and/or atomic interdiffusion layers at Co<sub>2</sub>YZ/GaAs or Co<sub>2</sub>YZ/Ge heterojunctions.<sup>28–30</sup>

### Epitaxial growth of Co<sub>2</sub>YZ films on GaAs and Ge

**Figure 2a–b** shows structural models illustrating the orientations for epitaxial crystal growth of Co<sub>2</sub>YZ films on GaAs and on Ge, respectively. Because there is almost no lattice mismatch between some of the Co<sub>2</sub>YZ compounds (0.564–0.570 nm) and GaAs or Ge (~0.566 nm), it is possible to realize epitaxial growth of the Co<sub>2</sub>YZ films. For the GaAs(001) surface highlighted by the blue square in **Figure 2a**, the

growth of Co<sub>2</sub>YZ films has been explored by low-temperature MBE methods.<sup>28,29</sup> Thus far, epitaxial growth of Co<sub>2</sub>MnGe,<sup>35</sup> Co<sub>2</sub>FeSi,<sup>36–39</sup> Co<sub>2</sub>FeAl,<sup>40–42</sup> Co<sub>2</sub>CrAl,<sup>40,43</sup> and Co<sub>2</sub>MnSi<sup>39,44,45</sup> films has been reported. The *B*<sub>2</sub>- or *L*<sub>21</sub>-Co<sub>2</sub>YZ/GaAs heterostructures formed at low temperatures from 100°C to 487°C enable electrical spin injection into GaAs through the Co<sub>2</sub>YZ/GaAs Schottky-tunnel barrier.<sup>35,37–39,44,45</sup> Owing to highly efficient spin injection and detection through the *B*<sub>2</sub>- or *L*<sub>21</sub>-ordered Co<sub>2</sub>YZ/GaAs interface, room-temperature spin transport was observed even in GaAs-based channels,<sup>39,45,46</sup> which are influenced by D'yakonov-Perel' spin relaxation due to the broken space inversion symmetry in the crystal structure. Progress in spin injection is described in the next section.

For Ge, on the other hand, we explored the epitaxial growth of Co<sub>2</sub>YZ films on the (111) surface shown by the blue triangle in **Figure 2b** using low-temperature MBE.<sup>47–51</sup> If we look at the (111) planes, we find that there is good matching between the atomic arrangements of Co<sub>2</sub>YZ and Ge.<sup>30</sup> The Ge(111) plane has also been utilized for the epitaxial growth of Fe-

based Heusler compounds<sup>52–56</sup> and all-Heusler-compound trilayers.<sup>57</sup> Epitaxial growth of Ge(111) layers on Heusler-compound structures was also demonstrated using low-temperature MBE methods.<sup>58,59</sup>

**Figure 2c** displays a reflection high-energy electron diffraction (RHEED) pattern observed during the growth of a Co<sub>2</sub>FeAl<sub>0.5</sub>Si<sub>0.5</sub> film on a Ge(111) surface, where the growth temperature is less than 100°C.<sup>51</sup> The symmetrical streak patterns show that two-dimensional epitaxial growth of the Co<sub>2</sub>FeAl<sub>0.5</sub>Si<sub>0.5</sub> film occurs on Ge(111). Structural and magnetic characterization revealed the formation of *B*<sub>2</sub>-ordered Co<sub>2</sub>FeAl<sub>0.5</sub>Si<sub>0.5</sub>/Ge(111) heterointerfaces despite the

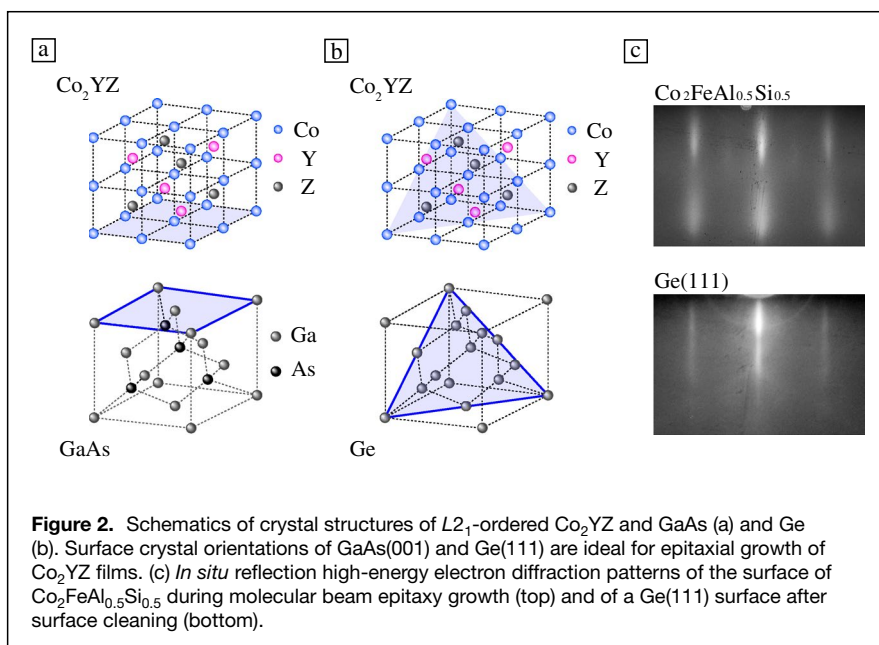


**Figure 2.** Schematics of crystal structures of *L*<sub>21</sub>-ordered Co<sub>2</sub>YZ and GaAs (a) and Ge (b). Surface crystal orientations of GaAs(001) and Ge(111) are ideal for epitaxial growth of Co<sub>2</sub>YZ films. (c) *In situ* reflection high-energy electron diffraction patterns of the surface of Co<sub>2</sub>FeAl<sub>0.5</sub>Si<sub>0.5</sub> during molecular beam epitaxy growth (top) and of a Ge(111) surface after surface cleaning (bottom).

low growth temperature.<sup>51,60</sup> Through these efforts, we have demonstrated the epitaxial growth of Co<sub>2</sub>FeAl<sub>x</sub>Si<sub>1-x</sub> films on Ge(111) at growth temperatures less than 100°C.<sup>51</sup>

Atomic-resolution high-angle annular dark-field (HAADF) scanning transmission electron microscopy (STEM) analyses of the Co<sub>2</sub>FeAl<sub>0.5</sub>Si<sub>0.5</sub> film grown on Ge(111) were also performed,<sup>60,61</sup> where the contrast in the HAADF-STEM image provides information on the mass distribution in the matrix and is related to the atomic number of each element. As shown in **Figure 3a**, the different crystallographic structures of Co<sub>2</sub>FeAl<sub>0.5</sub>Si<sub>0.5</sub> and Ge indicate the structural abruptness of the interface and the epitaxial relationship between the layers. However, there are some fluctuations in the atomic composition in the Co<sub>2</sub>FeAl<sub>0.5</sub>Si<sub>0.5</sub> layer near the interface, as denoted by arrows. These fluctuations are attributed to Ge out-diffusion during growth.<sup>60,61</sup> To suppress Ge out-diffusion near the interface, we recently developed a new method for improving the quality of the Co<sub>2</sub>FeAl<sub>0.5</sub>Si<sub>0.5</sub> layer. By inserting a very thin (~0.7 nm) Fe layer between Co<sub>2</sub>FeAl<sub>0.5</sub>Si<sub>0.5</sub> and Ge,<sup>62</sup> the compositional fluctuation due to out-diffusion of Ge atoms into the Co<sub>2</sub>FeAl<sub>0.5</sub>Si<sub>0.5</sub> layer is markedly suppressed (**Figure 3b**). As a result, B<sub>2</sub>-ordered Co<sub>2</sub>FeAl<sub>0.5</sub>Si<sub>0.5</sub> was formed near the interface on top of the Fe-terminated Ge layer (**Figure 3c**).<sup>62</sup> Recent progress in this effort on spin transport in Ge is also described later.

Thus far, it has been difficult to form B<sub>2</sub>- or L<sub>2</sub><sub>1</sub>-ordered Co<sub>2</sub>MnSi on Ge(111) even by low-temperature MBE methods.<sup>48,49</sup> To obtain a sufficient magnetic moment in Co<sub>2</sub>MnSi films on Ge(111), postannealing treatments were required.<sup>49,63,64</sup> While B<sub>2</sub>- or L<sub>2</sub><sub>1</sub>-ordered Co<sub>2</sub>MnSi was formed on Ge(111) after postannealing, it was still difficult to obtain high-quality and smooth Co<sub>2</sub>MnSi/Ge(111) heterojunctions due to atomic interdiffusion between Co<sub>2</sub>MnSi and Ge.<sup>49,63,64</sup> Although the contact resistance between Co<sub>2</sub>MnSi and Ge was relatively high, the insertion of an MgO tunnel-barrier layer at the interface was employed to obtain L<sub>2</sub><sub>1</sub>-ordered Co<sub>2</sub>MnSi on Ge.<sup>65</sup> Very recently, we predicted the formation of energetically stable Co<sub>2</sub>MnSi–Ge(111)

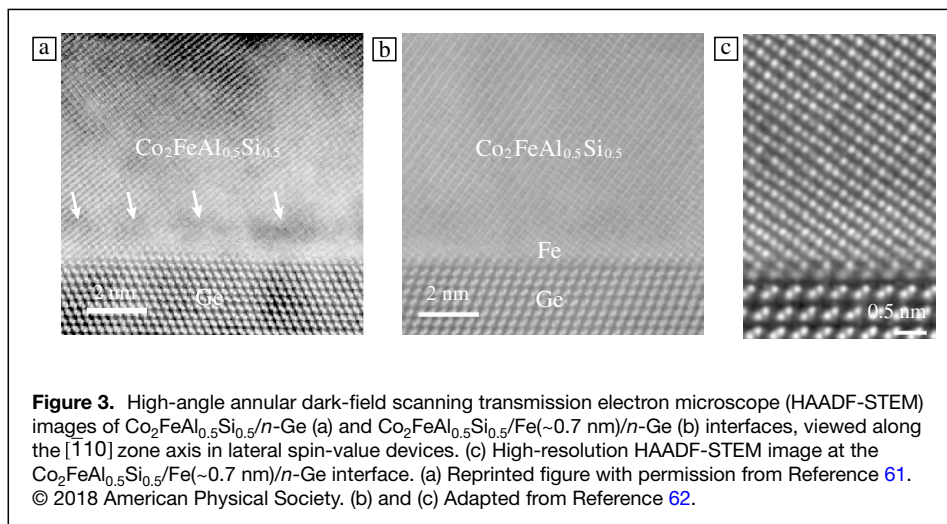
heterointerfaces with Fe atomic layers.<sup>66</sup> As expected, we demonstrated L<sub>2</sub><sub>1</sub>-ordered Co<sub>2</sub>MnSi films on Ge(111) using low-temperature MBE (~80°C). Owing to this effort and phosphorus (P) δ-doping techniques,<sup>30,67</sup> we decreased the contact resistance area product (*RA*) of the Co<sub>2</sub>MnSi/Ge Schottky-tunnel barrier down to ~0.1 kΩμm<sup>2</sup>,<sup>66</sup> resulting in a reduction of the parasitic resistance in the device structure.

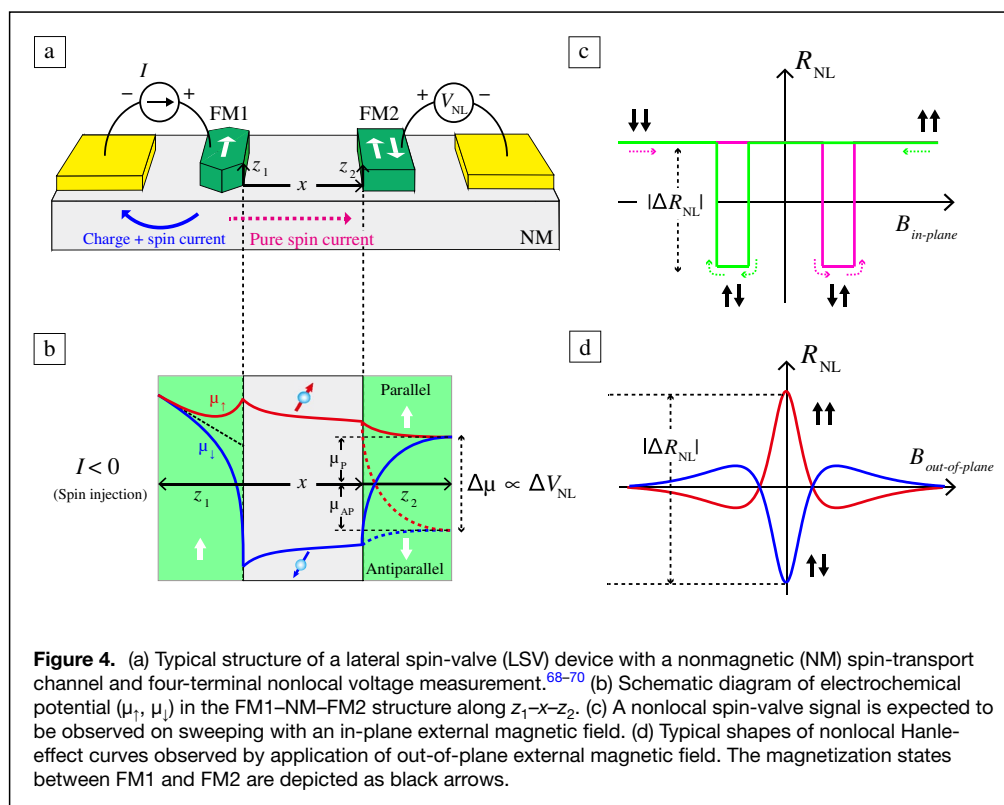
### Spin injection into GaAs and Ge with Co<sub>2</sub>YZ contacts

To evaluate electrical spin injection from FMs into nonmagnets (NMs), four-terminal nonlocal voltage measurements of lateral spin-valve (LSV) devices have been utilized in the research field of spintronics,<sup>68–70</sup> where charge-related magnetoresistance such as anisotropic magnetoresistance (AMR) and/or local Hall effects can be neglected. **Figure 4** shows a schematic illustration of the principles of the detection scheme for the nonlocal spin signal. A typical structure of an FM1–NM–FM2 LSV device is depicted in **Figure 4a**. If electrical spin injection can be realized under the application of a negative direct current (*I*), nonequilibrium splitting of electrochemical potentials,  $\Delta\mu = \mu_{\uparrow} - \mu_{\downarrow}$ , beneath the spin-injector contact (FM1) can be created. Here the created  $\Delta\mu$  is termed spin accumulation in NMs. As a result, the spin accumulation created in NMs can be detected as a pure spin current, a flow of spin angular momentum without charge currents, at the side of the spin-detector contact (FM2). **Figure 4b** shows a schematic illustration of  $\Delta\mu$  in the FM1–NM–FM2 structure. Along the lateral direction *x*, the exponentially decayed  $\Delta\mu$  is detected electrically as a difference in the nonlocal voltage ( $\Delta V_{\text{NL}}$ ) between parallel and antiparallel magnetization states. By sweeping the in-plane external magnetic field along the long axis of the FM1 and FM2 contacts, hysteretic nonlocal resistance changes ( $\Delta R_{\text{NL}} = \Delta V_{\text{NL}}/I$ ) are observed depending on the magnetization states between FM1 and FM2 (**Figure 4c**). In addition, by applying an out-of-plane external magnetic field to the LSV devices, the Hanle effect, which corresponds to Larmor spin precession in NMs, is also detected electrically.

For both parallel and antiparallel magnetization states, precessional decay of the nonlocal resistance is seen, as shown in **Figure 4d**. Based on fitting with the one-dimensional spin drift–diffusion model,<sup>69,71</sup> the spin relaxation mechanism in NMs can be roughly investigated.

The four-terminal nonlocal spin signals are recognized as evidence of the electrical detection of a pure spin current in the field of semiconductor spintronics.





In 2007, Lou et al. simultaneously observed nonlocal spin signals and Hanle-effect curves at low temperatures in *n*-type GaAs (*n*-GaAs) LSV devices with epitaxial Fe Schottky-tunnel contacts.<sup>71</sup> Since this development, electrical spin injection from Co<sub>2</sub>FeSi or Co<sub>2</sub>MnSi into GaAs has been investigated in LSV devices.<sup>38,39,44,45</sup> In particular, room-temperature nonlocal spin signals were observed in *n*-GaAs by using Co<sub>2</sub>FeSi/GaAs and Co<sub>2</sub>MnSi/CoFe/GaAs Schottky-tunnel contacts,<sup>39,45</sup> although nonlocal Hanle curves were not exhibited at room temperature. Because the magnitude of the nonlocal Hanle signal with a parallel or an antiparallel magnetization state is less than half the magnitude of the nonlocal spin signal ( $|\Delta R_{NL}|$ ) (Figure 4c–d), it is generally difficult to detect the nonlocal Hanle curves with both parallel and antiparallel magnetization states at room temperature in the case of small  $\Delta R_{NL}$  values.

For *n*-GaAs, it is particularly important to understand the influence of Co<sub>2</sub>YZ/GaAs Schottky-tunnel contacts and/or the D'yakonov-Perel' spin relaxation mechanism on the spin-transport signals. In 2014, Ebina et al. reported that insertion of a 1.3-nm-thick CoFe layer suppresses the diffusion of Mn atoms into GaAs during the growth of Co<sub>2</sub>MnSi films, leading to improved spin injection properties.<sup>45</sup> Then, Uemura et al. demonstrated nuclear-spin-based qubits in GaAs without using a large magnetic field because the efficient spin injection from Co<sub>2</sub>MnSi/CoFe contacts enabled dynamic nuclear polarization of Ga and As nuclei.<sup>72</sup> In 2016, Peterson et al. clarified the strong influence of D'yakonov-Perel' spin relaxation in *n*-GaAs in LSV devices with Co<sub>2</sub>FeSi and Co<sub>2</sub>MnSi contacts

from low temperatures up to room temperature.<sup>39</sup> However, in 2018, Rath et al. proposed that interfacial Mn segregation in Co<sub>2</sub>MnSi/GaAs(001) induces the loss of half-metallicity for the Co<sub>2</sub>MnSi film, leading to degradation of the performance of LSV devices.<sup>73</sup> Namely, it is inferred that the interfacial quality of Co<sub>2</sub>YZ/GaAs heterojunctions influences the ability to study room-temperature spin transport with nonlocal Hanle curves in both the parallel and antiparallel magnetization states. In 2019, Lin et al. used AlGaAs/GaAs-based two-dimensional electron gas (2DEG) systems with Co<sub>2</sub>MnSi contacts. Although they observed nonlocal spin signals up to room temperature, the spin relaxation mechanism could not be explained clearly.<sup>46</sup> These efforts have revealed the effectiveness of the use of Co<sub>2</sub>YZ/*n*-GaAs Schottky-tunnel contacts to study spin injection, transport, and detection in *n*-GaAs.

Because of the space inversion symmetry in Ge, the influence of the D'yakonov-Perel' mechanism on spin relaxation is negligibly small in Ge channels. If highly efficient spin injection from Co<sub>2</sub>YZ films into Ge is demonstrated, efficient spin transport can be expected even in Ge-based LSV devices. Thus far, for *n*-type Ge (*n*-Ge), a modified Elliott–Yafet spin relaxation mechanism including the spin–orbit interaction of host materials and donor atoms has been verified theoretically<sup>74,75</sup> and in experiments.<sup>51,76–78</sup> To explore the lateral spin transport, we prepared LSV devices with an *n*-Ge spin-transport channel and two ferromagnetic Co<sub>2</sub>YZ contacts,<sup>51,62,76–80</sup> as shown in Figure 5a. The detailed growth and fabrication processes for the LSV device were as follows: First, an undoped

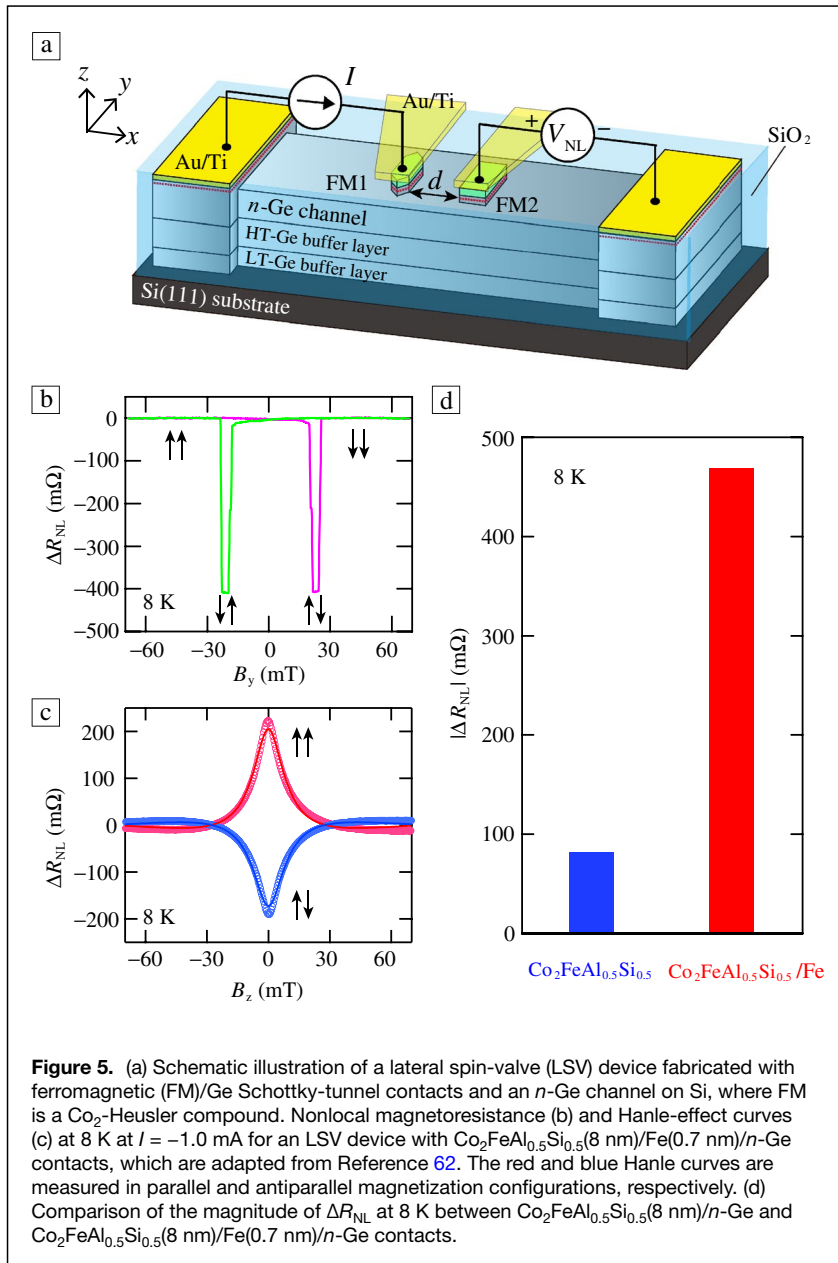


**Figure 5.** (a) Schematic illustration of a lateral spin-valve (LSV) device fabricated with ferromagnetic (FM)/Ge Schottky-tunnel contacts and an *n*-Ge channel on Si, where FM is a Co<sub>2</sub>-Heusler compound. Nonlocal magnetoresistance (b) and Hanle-effect curves (c) at 8 K for  $I = -1.0$  mA for an LSV device with Co<sub>2</sub>FeAl<sub>0.5</sub>Si<sub>0.5</sub>(8 nm)/Fe(0.7 nm)/*n*-Ge contacts, which are adapted from Reference 62. The red and blue Hanle curves are measured in parallel and antiparallel magnetization configurations, respectively. (d) Comparison of the magnitude of  $\Delta R_{NL}$  at 8 K between Co<sub>2</sub>FeAl<sub>0.5</sub>Si<sub>0.5</sub>(8 nm)/*n*-Ge and Co<sub>2</sub>FeAl<sub>0.5</sub>Si<sub>0.5</sub>(8 nm)/Fe(0.7 nm)/*n*-Ge contacts.

Ge(111) buffer layer (~28 nm) (LT-Ge) was grown at 350°C on a commercial undoped Si(111) substrate ( $\rho \sim 1000 \Omega \text{ cm}$ ), followed by an undoped Ge(111) buffer layer (~70 nm) grown at 700°C (HT-Ge), where we utilized a two-step MBE growth technique.<sup>81</sup> Next, as the spin-transport layer, a 140-nm-thick P-doped Ge(111) layer (doping concentration  $\sim 10^{19} \text{ cm}^{-3}$ ) was grown on top by MBE at 350°C. Here, the room-temperature carrier (electron) concentration of the spin-transport layer is  $6.0\text{--}7.0 \times 10^{18} \text{ cm}^{-3}$ ,<sup>62,66,80</sup> estimated from Hall effect measurements. To eliminate the large conductivity mismatch<sup>82–85</sup> between Co<sub>2</sub>YZ and *n*-Ge, we developed a Schottky-tunnel contact consisting of Co<sub>2</sub>YZ and a P  $\delta$ -doped Ge layer,<sup>30,67</sup> where the P  $\delta$ -doped Ge layer was terminated

by a 0.7-nm-thick Fe layer.<sup>62,66,80</sup> After that, a Co<sub>2</sub>YZ film was grown on top by MBE at a growth temperature of less than 100°C.<sup>30,51,66</sup> Thus, the whole sample stack was prepared by MBE techniques. Finally, the formed Co<sub>2</sub>YZ/*n*-Ge Schottky-tunnel layer was patterned into two contacts with a width of 0.4  $\mu\text{m}$  (FM1) or 0.5  $\mu\text{m}$  (FM2), and a channel structure with a channel width ( $w$ ) of 5.0  $\mu\text{m}$  and an edge-to-edge distance ( $d$ ) between the FM contacts of 0.45  $\mu\text{m}$ . The detailed fabrication processes for the LSV device are presented in the literature.<sup>79</sup>

Figure 5b shows a representative  $\Delta R_{NL}$  signal as a function of the in-plane magnetic field ( $B_y$ ) at  $I = -1.0$  mA at 8 K for an LSV device with Co<sub>2</sub>FeAl<sub>0.5</sub>Si<sub>0.5</sub>(8 nm)/Fe(0.7 nm)/*n*-Ge Schottky-tunnel contacts as shown in Figure 3c. Here, a negative value of  $I$  ( $I < 0$ ) indicates that the spin-polarized electrons are injected into *n*-Ge from Co<sub>2</sub>FeAl<sub>0.5</sub>Si<sub>0.5</sub> (i.e., a spin injection condition via the Schottky-tunnel barrier). An evident nonlocal hysteresis curve is observed, which depends on the parallel and antiparallel magnetization states between Co<sub>2</sub>FeAl<sub>0.5</sub>Si<sub>0.5</sub> contacts, depicted by the arrows in Figure 5b. Notably, the value of  $\Delta R_{NL}$  reaches  $\sim 400$  m $\Omega$ . In four-terminal nonlocal measurements under an out-of-plane magnetic field ( $B_z$ ), we also observe nonlocal Hanle curves, indicating spin precession in the channel (Figure 5c). We also note that, even in the antiparallel magnetization state under the application of  $B_z$ , the Hanle-effect signal is clearly observed, indicating reliable pure-spin-current transport in the *n*-Ge

layer. Using a one-dimensional spin drift–diffusion model,<sup>69,71</sup> the spin injection/detection efficiency and spin lifetime can be roughly estimated to be  $\sim 0.24$  and  $\sim 0.76$  ns, respectively, from the four-terminal nonlocal spin-transport data. For comparison, we explored four-terminal nonlocal spin-transport data for LSV devices with various FM Schottky-tunnel contacts.<sup>30,51,76</sup> In Figure 5d, we give a simple comparison of the magnitude of  $\Delta R_{NL}$  at 8 K for LSV devices with Co<sub>2</sub>FeAl<sub>0.5</sub>Si<sub>0.5</sub>(8 nm)/*n*-Ge (blue) and Co<sub>2</sub>FeAl<sub>0.5</sub>Si<sub>0.5</sub>(8 nm)/Fe(0.7 nm)/*n*-Ge (red) Schottky-tunnel contacts. The magnitude of  $\Delta R_{NL}$  is significantly enhanced only by inserting a 0.7-nm-thick Fe layer between Co<sub>2</sub>FeAl<sub>0.5</sub>Si<sub>0.5</sub> and *n*-Ge. This feature is strongly related to the interface quality as shown in Figure 3. For

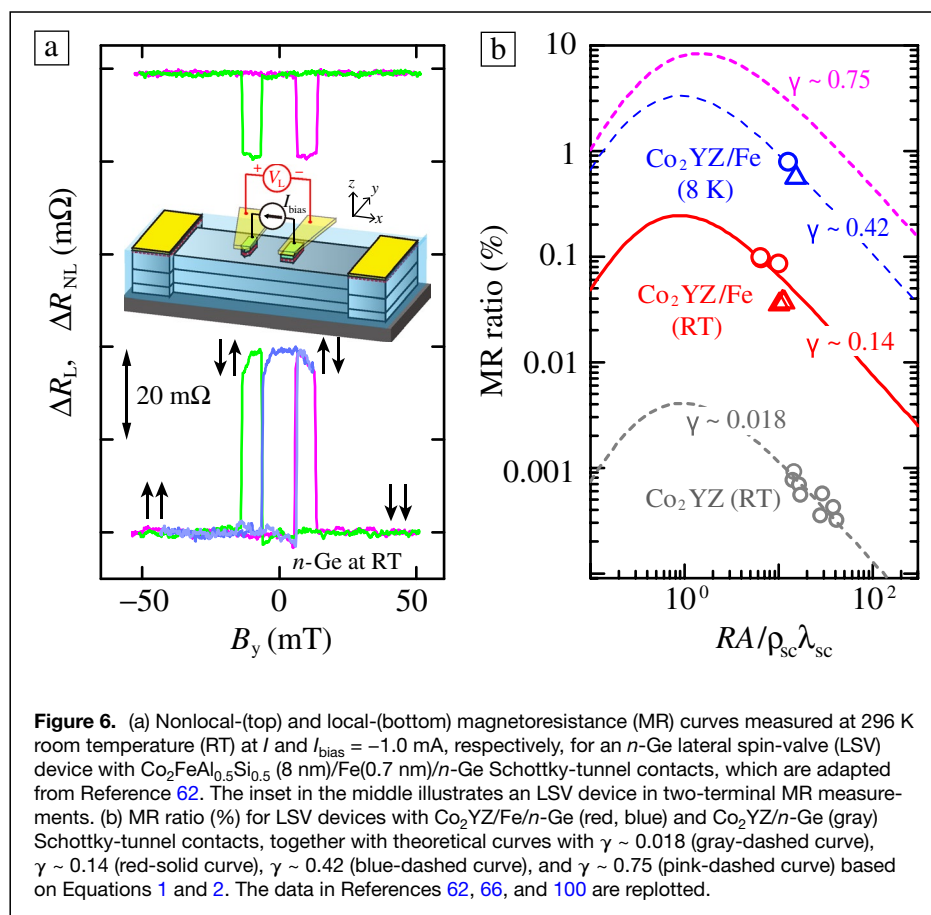
reference, if Co<sub>2</sub>FeAl<sub>0.5</sub>Si<sub>0.5</sub> contacts were not used in the *n*-Ge-based LSV devices, we could not obtain such large  $\Delta R_{NL}$  values. For example, when we used epitaxial CoFe/*n*-Ge Schottky-tunnel contacts, the magnitude of  $\Delta R_{NL}$  was less than 4 m $\Omega$ , which is two orders of magnitude smaller than that in Figure 5b. Therefore, the use of Co<sub>2</sub>YZ is clearly effective even for Ge-based spintronic devices, but it is quite important to achieve a high-quality heterointerface between Co<sub>2</sub>YZ and Ge,<sup>30,51,61,62,66</sup> as well as GaAs.<sup>45,73</sup>

### Potential for applications

Room-temperature pure-spin-current transport with Hanle curves was first observed in LSV devices with semiconducting graphene<sup>86–88</sup> and Si<sup>89–91</sup> channels because of the large spin diffusion lengths ( $\lambda_{SC}$ ) of several microns even at room temperature. Then, progress in the crystal growth and formation of high-quality Co<sub>2</sub>YZ/Ge heterojunctions also enabled pure-spin-current transport with Hanle curves at room temperature even in Ge-based LSV devices,<sup>92</sup> despite a relatively small  $\lambda_{SC}$  (~0.4  $\mu$ m) compared to graphene and Si. In this section, we discuss the potential use of Co<sub>2</sub>YZ/Ge structures in practical applications.

It is generally important to observe a two-terminal local magnetoresistance (MR) effect, indicating spin-dependent transport of spin-polarized electrons or holes through semiconductors at room temperature (RT).<sup>31–34</sup> The two-terminal MR ratio is defined as  $(\Delta R_L/R_p) \times 100$ , where  $\Delta R_L$  and  $R_p$  are the two-terminal local spin accumulation signal ( $\Delta V_L/I_{bias}$ ), shown in the inset (middle) of Figure 6a, and the resistance between the FM contacts through the semiconductor layer in the parallel magnetization state, respectively. In Si-based LSV devices,<sup>91,93–96</sup> tunnel barriers consisting of insulators such as MgO were found to cause a large parasitic resistance component in  $R_p$ . As a result, to obtain an MR of 0.06% at room temperature, which is the largest value in Si LSV devices, quite high bias voltages (~2.3 V) must be applied, leading to a large S/D voltage and electric power of ~1.15 mW.<sup>96</sup> Thus, the use of controllable Schottky-tunnel contacts should be explored to reduce the electric power required to obtain the two-terminal MR effect.

To overcome the issue of limitations due to high bias voltages, we focused on achieving a high-quality Co<sub>2</sub>YZ/Fe/Ge heterointerface, shown in Figures 3 and 5, for the Schottky-tunnel contacts in the LSV devices with *n*-Ge. Thanks to P  $\delta$ -doping techniques,<sup>30,67</sup> the *RA* value could be reduced to ~0.1 k $\Omega$   $\mu$ m<sup>2</sup> at room temperature.<sup>62,66,80</sup> The bottom of Figure 6a shows a two-terminal local spin signal ( $\Delta R_L = \Delta V_L/I_{bias}$ ) as a function of  $B_y$  at  $I_{bias} = -1.0$  mA at 296 K. As a reference, the corresponding  $\Delta R_{NL}$  as a function of  $B_y$  at  $I = -1.0$  mA at 296 K is also shown at the top. Positive changes in  $\Delta R_L$  with hysteretic behavior are clearly observed even at room temperature.<sup>62,66</sup> The blue curve at the bottom represents a minor loop with abrupt magnetization switching between parallel and antiparallel states, implying that the observed positive  $\Delta R_L$  is derived from conventional spin-dependent transport of electrons through the *n*-Ge layer. From these data for various LSV devices, we have roughly estimated the MR ratio to be 0.04–0.1% at room temperature.<sup>62,66</sup> Notably, the data were obtained at low applied bias voltages (~0.12 V), leading to a decrease in the electric power required to ~0.12 mW, one order of magnitude lower than that (~1.15 mW) for Si-based LSV devices with MgO tunnel barriers.<sup>96</sup> Although the MR ratio for Co<sub>2</sub>YZ/Fe/*n*-Ge LSV devices is higher than that for Si-based LSV devices,<sup>91,93–96</sup> there is still a great gap



between this and the MR values required for logic/memory applications with a spin-MOSFET.<sup>34</sup> We discuss a strategy for achieving high-performance Ge-based LSV devices, together with experimental results and theoretical predictions in the following section.

Given the definition of the MR ratio as  $(\Delta R_L/R_p) \times 100$ , we should separately determine the values of  $\Delta R_L$  and  $R_p$ . In general, on the basis of the one-dimensional spin drift–diffusion model developed by Fert and Jaffrès,<sup>84</sup> the magnitude of  $\Delta R_L$  and  $R_p$  in FM–SC–FM with double tunnel barriers has been expressed as follows.<sup>84,94,97–99</sup>

$$\Delta R_L = \frac{8\gamma^2 r_b^2 r_{SC}}{S_{SC} \left[ (2r_b + r_{SC})^2 \exp\left(\frac{d}{\lambda_{SC}}\right) - r_{SC}^2 \exp\left(-\frac{d}{\lambda_{SC}}\right) \right]}, \quad 1$$

$$R_p = \frac{1}{S_{SC}} \left[ r_{SC} \frac{d}{\lambda_{SC}} + 2(1 - \gamma^2)r_b + 2 \frac{\gamma^2 r_{SC} r_b \tanh\left(\frac{d}{2\lambda_{SC}}\right)}{r_b + r_{SC} \tanh\left(\frac{d}{2\lambda_{SC}}\right)} \right], \quad 2$$

where  $\gamma$  is the spin polarization of the FM/SC interfaces,  $r_b$  is the value of  $RA$  for the FM/SC contacts,  $S_{SC}$  is the cross-sectional area of the SC spin-transport channel, and  $r_{SC}$  ( $= \rho_{SC} \times \lambda_{SC}$ ) is the spin resistance of the SC layer. Here, for our Ge-based LSV devices,  $d$  ( $= 0.35$ – $0.45 \mu\text{m}$ ) and  $S_{SC}$  ( $= 0.98 \mu\text{m}^2$ ) are device parameters, and  $\rho_{SC}$  is the channel resistivity ( $1.59 \text{ m}\Omega \text{ cm} \leq \rho_{SC} \leq 2.16 \text{ m}\Omega \text{ cm}$ ). The  $RA$  values ( $0.1$ – $0.4 \text{ k}\Omega \mu\text{m}^2$ ) were directly measured by a three-terminal method, as described in previous work.<sup>62</sup> Since the value of  $\lambda_{SC}$  has already been estimated at 8 K ( $= 0.84 \pm 0.07 \mu\text{m}$ )<sup>62,77</sup> and 296 K ( $= 0.44 \pm 0.02 \mu\text{m}$ ),<sup>92</sup> we can roughly estimate the value of  $r_{SC}$  at each temperature.

Figure 6b shows plots of the MR ratio as a function of  $r_b/r_{SC}$  ( $= RA/\rho_{SC}\lambda_{SC}$ ) for Co<sub>2</sub>YZ/*n*-Ge and Co<sub>2</sub>YZ/Fe/*n*-Ge LSV devices, and theoretical curves based on Equations 1 and 2. Here, the gray plots are data at 296 K for Co<sub>2</sub>FeAl/*n*-Ge LSV devices in Reference 100 and the red plots are examples for Co<sub>2</sub>MnSi/Fe/*n*-Ge (circles) at 297 K<sup>66</sup> and for Co<sub>2</sub>FeAl<sub>0.5</sub>Si<sub>0.5</sub>/Fe/*n*-Ge (triangles) at 296 K.<sup>62</sup> As references, we also show the data for Co<sub>2</sub>MnSi/Fe/*n*-Ge (circles) at 8 K and for Co<sub>2</sub>FeAl<sub>0.5</sub>Si<sub>0.5</sub>/Fe/*n*-Ge (triangles) at 8 K in blue. Furthermore, to discuss the present situation, we provide theoretical curves with  $\gamma \sim 0.018$  (gray-dashed curve),  $\gamma \sim 0.14$  (red-solid curve),  $\gamma \sim 0.42$  (blue-dashed curve), and  $\gamma \sim 0.75$  (pink-dashed curve) based on Equations 1 and 2. Comparison of experimental data and theoretical curves shows that the interface spin polarization  $\gamma$  is enhanced by an order of magnitude owing to the contribution from high-quality Co<sub>2</sub>YZ/Fe/Ge Schottky-tunnel contacts. Notably, the MR ratio can be enhanced up to  $\sim 1\%$  at 8 K because of the increase in  $\gamma$  ( $\sim 0.42$ ). If a large  $\gamma$  ( $0.4$ – $0.5$ ) is demonstrated at room temperature, an MR ratio of more than 1% can be obtained even for LSV devices with *n*-Ge. Assuming  $\gamma \sim 0.75$ , the MR ratio can reach 10%. Thus, half-metallic Co<sub>2</sub>YZ is effective for obtaining sizable MR ratios in LSV devices with *n*-Ge. However, as

with MTJs,<sup>7–9</sup> the temperature dependence of the half-metallicity should be improved in Co<sub>2</sub>YZ/Fe/*n*-Ge Schottky-tunnel contacts.<sup>80,101</sup>

Even if we achieve  $\gamma \sim 0.9$ , the MR ratio could not reach a value greater than 100%, which is required to use a Ge-spin-MOSFET for spin-based logic/memory applications.<sup>34</sup> In this case, the limitation of MR enhancement depends strongly on having a small value of  $\lambda_{SC}$  for *n*-Ge at room temperature. As previously mentioned, the present value of  $\lambda_{SC}$  for the *n*-Ge spin-transport channel used here is  $0.84 \pm 0.07 \mu\text{m}$  at 8 K<sup>77</sup> and  $0.44 \pm 0.02 \mu\text{m}$  at room temperature.<sup>92</sup> It should be emphasized that an increase in  $\lambda_{SC}$  to more than  $2 \mu\text{m}$  at room temperature enables enhancement of the MR ratio of more than 100%. For *n*-Ge, intervalley spin-flip scattering of electrons between *L* valleys in the conduction band should be taken into account to increase  $\lambda_{SC}$ .<sup>51,74–78</sup> Recently, impurity- and phonon-induced intervalley spin-flip scattering processes were partly suppressed by utilizing a strained *n*-Si<sub>0.1</sub>Ge<sub>0.9</sub>(111) layer,<sup>102,103</sup> where the Ge-rich Si<sub>1–*x*</sub>Ge<sub>*x*</sub> exhibited a Ge-like electronic band structure with conduction-band minima at *L* points. In the future, researchers should explore the simultaneous utilization of high-quality Co<sub>2</sub>YZ/Fe/Ge Schottky-tunnel contacts with a large  $\gamma$  ( $\geq 0.8$ ) and strained *n*-Ge-rich Si<sub>1–*x*</sub>Ge<sub>*x*</sub> channels with a large  $\lambda_{SC}$  ( $\geq 2.0 \mu\text{m}$ ) at room temperature.

## Conclusion

This article reviewed the progress of the GaAs- and Ge-based semiconductor spintronics with ferromagnetic Co<sub>2</sub>-Heusler compounds showing high spin polarization. The GaAs(001) and Ge(111) surface orientations have been utilized for epitaxial growth of Co<sub>2</sub>-Heusler films using low-temperature MBE. Experimental studies of electrical spin injection from Co<sub>2</sub>-Heusler contacts into GaAs and Ge through Schottky-tunnel barriers at room temperature have been reported, meaning that Co<sub>2</sub>-Heusler compounds are useful for realizing spin injection, transport, and detection in GaAs and Ge. However, to achieve highly efficient spin-transport properties, it is important to suppress the interfacial out-diffusion of GaAs or Ge into the Co<sub>2</sub>-Heusler layer near the heterojunctions. Recent progress in high-quality Co<sub>2</sub>-Heusler/Ge heterojunctions has demonstrated two-terminal magnetoresistance ratios of more than 0.1% at room temperature even for semiconductor spintronic device structures. This approach using Co<sub>2</sub>-Heusler compounds provides a powerful solution to the need for simultaneous achievement of highly efficient spin injection and low electric power at the source and drain contacts in semiconductor devices such as spin MOSFETs.

## Acknowledgments

We acknowledge K. Sawano, S. Yamada, K. Kudo, M. Tsukahara, T. Naito, Y. Wagatsuma, B. Kuerbanjiang, T. Oguchi, R. Nakatani, V. K. Lazarov, Y. Shiratsuchi, T. Fukushima, F. Kuroda, and S. Honda for useful discussions and experimental support. We also acknowledge financial support from JSPS

KAKENHI (Grant Nos. 19H05616, 19H02175, 21H05000), JST PRESTO (Grant No. JPMJPR20BA), and the Spintronics Research Network of Japan (Spin-RNJ).

### Data availability

The data that support the findings of this study are available from the corresponding author upon reasonable request.

### Conflict of interest

The authors declare that they have no conflict of interest.

### Open Access

This article is licensed under a Creative Commons Attribution 4.0 International License, which permits use, sharing, adaptation, distribution and reproduction in any medium or format, as long as you give appropriate credit to the original author(s) and the source, provide a link to the Creative Commons license, and indicate if changes were made. The images or other third party material in this article are included in the article's Creative Commons license, unless indicated otherwise in a credit line to the material. If material is not included in the article's Creative Commons license and your intended use is not permitted by statutory regulation or exceeds the permitted use, you will need to obtain permission directly from the copyright holder. To view a copy of this license, visit <http://creativecommons.org/licenses/by/4.0/>.

### References

1. I. Galanakis, P.H. Dederichs, N. Papanikolaou, *Phys. Rev. B* **66**, 174429 (2002)
2. K. Inomata, N. Ikeda, N. Tezuka, R. Goto, S. Sugimoto, M. Wojcik, E. Jedryka, *Sci. Technol. Adv. Mater.* **9**, 014101 (2008)
3. B. Balke, S. Wurmehl, G.H. Fecher, C. Felser, J. Kübler, *Sci. Technol. Adv. Mater.* **9**, 014102 (2008)
4. S. Bhatti, R. Sbiaa, A. Hirohata, H. Ohno, S. Fukami, S.N. Piramanayagam, *Mater. Today* **20**, 530 (2017)
5. S. Yuasa, K. Hono, G. Hu, D.C. Worledge, *MRS Bull.* **43**(5), 352 (2018)
6. K. Inomata, S. Okamura, R. Goto, N. Tezuka, *Jpn. J. Appl. Phys.* **42**, L419 (2003)
7. Y. Sakuraba, M. Hattori, M. Oogane, Y. Ando, H. Kato, A. Sakuma, T. Miyazaki, H. Kubota, *Appl. Phys. Lett.* **88**, 192508 (2006)
8. T. Ishikawa, S. Hakamata, K. Matsuda, T. Uemura, M. Yamamoto, *J. Appl. Phys.* **103**, 07A919 (2008)
9. H.-X. Liu, Y. Honda, T. Taira, K. Matsuda, M. Arita, T. Uemura, M. Yamamoto, *Appl. Phys. Lett.* **101**, 132418 (2012)
10. T. Iwase, Y. Sakuraba, S. Bosu, K. Saito, S. Mitani, K. Takanashi, *Appl. Phys. Express* **2**, 063003 (2009)
11. T.M. Nakatani, T. Furubayashi, S. Kasai, H. Sukegawa, Y.K. Takahashi, S. Mitani, K. Hono, *Appl. Phys. Lett.* **96**, 212501 (2010)
12. Y.K. Takahashi, A. Srinivasan, B. Varaprasad, A. Rajanikanth, N. Hase, T.M. Nakatani, S. Kasai, T. Furubayashi, K. Hono, *Appl. Phys. Lett.* **98**, 152501 (2011)
13. T. Furubayashi, K. Kodama, H. Sukegawa, Y.K. Takahashi, K. Inomata, K. Hono, *Appl. Phys. Lett.* **93**, 122507 (2008)
14. T. Kimura, N. Hashimoto, S. Yamada, M. Miyao, K. Hamaya, *NPG Asia Mater.* **4**, e9 (2012)
15. K. Hamaya, N. Hashimoto, S. Oki, S. Yamada, M. Miyao, T. Kimura, *Phys. Rev. B* **85**, 100404(R) (2012)
16. Y.K. Takahashi, S. Kasai, S. Hirayama, S. Mitani, K. Hono, *Appl. Phys. Lett.* **100**, 052405 (2012)
17. S.A. Wolf, D.D. Awschalom, R.A. Buhrman, J.M. Daughton, S. von Molnár, M.L. Roukes, A.Y. Chtchelkanova, D.M. Treger, *Science* **294**, 1488 (2001)
18. I. Žuti, J. Fabian, S.D. Sarma, *Rev. Mod. Phys.* **76**, 323 (2004)
19. S.A. Crooker, M. Furis, X. Lou, C. Adelmann, D.L. Smith, C.J. Palmström, P.A. Crowell, *Science* **309**, 2191 (2005)
20. D.D. Awschalom, M.E. Flatté, *Nat. Phys.* **3**, 153 (2007)
21. I. Appelbaum, B. Huang, D.J. Monsma, *Nature* **447**, 295 (2007)
22. H. Dery, P. Dalal, L. Cywiski, L.J. Sham, *Nature* **447**, 573 (2007)
23. H.C. Koo, J.H. Kwon, J. Eom, J. Chang, S.H. Han, M. Johnson, *Science* **325**(5947), 1515 (2009)
24. Y. Zhou, W. Han, L.-T. Chang, F. Xiu, M. Wang, M. Oehme, I.A. Fischer, J. Schulze, R.K. Kawakami, K.L. Wang, *Phys. Rev. B* **84**, 125323 (2011)
25. R. Jansen, *Nat. Mater.* **11**, 400 (2012)
26. P. Chuang, S.-C. Ho, L.W. Smith, F. Sfigakis, M. Pepper, C.-H. Chen, J.-C. Fan, J.P. Griffiths, I. Farrer, H.E. Beere, G.A.C. Jones, D.A. Ritchie, T.-M. Chen, *Nat. Nanotechnol.* **10**, 35 (2015)
27. W.Y. Choi, H.-J. Kim, J. Chang, S.H. Han, H.C. Koo, M. Johnson, *Nat. Nanotechnol.* **10**, 666 (2015)
28. C. Palmström, *MRS Bull.* **28**(10), 725 (2003)
29. R. Farshchi, M. Ramsteiner, *J. Appl. Phys.* **113**, 191101 (2013)
30. K. Hamaya, Y. Fujita, M. Yamada, M. Kawano, S. Yamada, K. Sawano, *J. Phys. D Appl. Phys.* **51**, 393001 (2018)
31. S. Datta, B. Das, *Appl. Phys. Lett.* **56**, 665 (1990)
32. S. Sugahara, M. Tanaka, *Appl. Phys. Lett.* **84**, 2307 (2004)
33. M. Tanaka, S. Sugahara, *IEEE Trans. Electron Devices* **54**, 961 (2007)
34. T. Tanamoto, H. Sugiyama, T. Inokuchi, T. Marukame, M. Ishikawa, K. Ikegami, Y. Saito, *J. Appl. Phys.* **109**, 07C312 (2011)
35. X.Y. Dong, C. Adelmann, J.Q. Xie, C.J. Palmström, X. Lou, J. Strand, P.A. Crowell, J.-P. Barnes, A.K. Petford-Long, *Appl. Phys. Lett.* **86**, 102107 (2005)
36. M. Hashimoto, J. Herfort, H.-P. Schönherr, K.H. Ploog, *Appl. Phys. Lett.* **87**, 102506 (2005)
37. M. Ramsteiner, O. Brandt, T. Flissikowski, H.T. Grahn, M. Hashimoto, J. Herfort, H. Kostial, *Phys. Rev. B* **78**, 121303(R) (2008)
38. P. Bruski, Y. Manzke, R. Farshchi, O. Brandt, J. Herfort, M. Ramsteiner, *Appl. Phys. Lett.* **103**, 052406 (2013)
39. T.A. Peterson, S.J. Patel, C.C. Geppert, K.D. Christie, A. Rath, D. Pennachio, M.E. Flatté, P.M. Voyles, C.J. Palmström, P.A. Crowell, *Phys. Rev. B* **94**, 235309 (2016)
40. A. Hirohata, H. Kurebayashi, S. Okamura, M. Kikuchi, T. Masaki, T. Nozaki, N. Tezuka, K. Inomata, *J. Appl. Phys.* **97**, 103714 (2005)
41. S. Qiao, S. Nie, J. Zhao, X. Zhang, *J. Appl. Phys.* **117**, 093904 (2015)
42. X. Zhang, W. Liu, Y. Yan, W. Niu, B. Lai, Y. Zhao, W. Wang, L. He, H. Meng, Y. Xu, *Appl. Phys. Lett.* **113**, 212401 (2018)
43. Y.V. Kudryavtsev, V.N. Uvarov, V.A. Oksenenko, Y.P. Lee, J.B. Kim, Y.H. Hyun, K.W. Kim, J.Y. Rhee, J. Dubowik, *Phys. Rev. B* **77**, 195104 (2008)
44. T. Akiho, J. Shan, H.-X. Liu, K. Matsuda, M. Yamamoto, T. Uemura, *Phys. Rev. B* **87**, 235205 (2013)
45. Y. Ebina, T. Akiho, H.-X. Liu, M. Yamamoto, T. Uemura, *Appl. Phys. Lett.* **104**, 172405 (2014)
46. Z. Lin, D. Pan, M. Rasly, T. Uemura, *Appl. Phys. Lett.* **114**, 012405 (2019)
47. K. Kasahara, K. Yamamoto, S. Yamada, T. Murakami, K. Hamaya, K. Mibu, M. Miyao, *J. Appl. Phys.* **107**, 09B105 (2010)
48. S. Yamada, K. Hamaya, T. Murakami, B. Varaprasad, Y.K. Takahashi, A. Rajanikanth, K. Hono, M. Miyao, *J. Appl. Phys.* **109**, 07B113 (2011)
49. M. Kawano, S. Yamada, S. Oki, K. Tanikawa, M. Miyao, K. Hamaya, *Jpn. J. Appl. Phys.* **52**, 04CM06 (2013)
50. K. Kasahara, Y. Fujita, S. Yamada, K. Sawano, M. Miyao, K. Hamaya, *Appl. Phys. Express* **7**, 033002 (2014)
51. Y. Fujita, M. Yamada, M. Tsukahara, T. Oka, S. Yamada, T. Kanashima, K. Sawano, K. Hamaya, *Phys. Rev. Appl.* **8**, 014007 (2017)
52. T. Sadoh, M. Kumano, R. Kizuka, K. Ueda, A. Kenjo, M. Miyao, *Appl. Phys. Lett.* **89**, 182511 (2006)



53. K. Ueda, K. Hamaya, K. Yamamoto, Y. Ando, T. Sadoh, Y. Maeda, M. Miyao, *Appl. Phys. Lett.* **93**, 112108 (2008)
54. K. Hamaya, H. Itoh, O. Nakatsuka, K. Ueda, K. Yamamoto, M. Itakura, T. Taniyama, T. Ono, M. Miyao, *Phys. Rev. Lett.* **102**, 137204 (2009)
55. K. Hamaya, T. Murakami, S. Yamada, K. Mibu, M. Miyao, *Phys. Rev. B* **83**, 144411 (2011)
56. S. Yamada, J. Sagar, S. Honda, L. Lari, G. Takemoto, H. Itoh, A. Hirohata, K. Mibu, M. Miyao, K. Hamaya, *Phys. Rev. B* **86**, 174406 (2012)
57. S. Yamada, S. Honda, J. Hirayama, M. Kawano, K. Santo, K. Tanikawa, T. Kanashima, H. Itoh, K. Hamaya, *Phys. Rev. B* **94**, 094435 (2016)
58. S. Yamada, K. Tanikawa, M. Miyao, K. Hamaya, *Cryst. Growth Des.* **12**, 4703 (2012)
59. M. Kawano, S. Yamada, K. Tanikawa, K. Sawano, M. Miyao, K. Hamaya, *Appl. Phys. Lett.* **102**, 121908 (2013)
60. Z. Nedelkoski, B. Kuerbanjiang, S.E. Glover, A. Sanchez, D. Kepaptsoglou, A. Ghasemi, C.W. Burrows, S. Yamada, K. Hamaya, Q.M. Ramasse, P. Hasnip, T. Hase, G. Bell, A. Hirohata, V. Lazarov, *Sci. Rep.* **6**, 37282 (2016)
61. B. Kuerbanjiang, Y. Fujita, M. Yamada, S. Yamada, A.M. Sanchez, P.J. Hasnip, A. Ghasemi, D. Kepaptsoglou, G. Bell, K. Sawano, K. Hamaya, V.K. Lazarov, *Phys. Rev. B* **98**, 115304 (2018)
62. M. Yamada, F. Kuroda, M. Tsukahara, S. Yamada, T. Fukushima, K. Sawano, T. Oguchi, K. Hamaya, *NPG Asia Mater.* **12**, 47 (2020)
63. M.A.I. Nahid, M. Oogane, H. Naganuma, Y. Ando, *Appl. Phys. Lett.* **96**, 142501 (2010)
64. M.A.I. Nahid, M. Oogane, H. Naganuma, Y. Ando, *Phys. Status Solidi A* **208**, 675 (2011)
65. G. Li, T. Taira, K. Matsuda, M. Arita, T. Uemura, M. Yamamoto, *Appl. Phys. Lett.* **98**, 262505 (2011)
66. K. Kudo, M. Yamada, S. Honda, Y. Wagatsuma, S. Yamada, K. Sawano, K. Hamaya, *Appl. Phys. Lett.* **118**, 162404 (2021)
67. M. Yamada, K. Sawano, M. Uematsu, K.M. Itoh, *Appl. Phys. Lett.* **107**, 132101 (2015)
68. M. Johnson, R.H. Silsbee, *Phys. Rev. Lett.* **55**, 1790 (1985)
69. F.J. Jedema, H.B. Heersche, A.T. Filip, J.J.A. Baselmans, B.J. van Wees, *Nature* (London) **416**(6882), 713 (2002)
70. T. Kimura, Y. Otani, *J. Phys. Condens. Matter* **19**, 165216 (2007)
71. X. Lou, C. Adelman, S.A. Crooker, E.S. Garlid, J. Zhang, K.S.M. Reddy, S.D. Flexner, C.J. Palmström, P.A. Crowell, *Nat. Phys.* **3**, 197 (2007)
72. T. Uemura, T. Akiho, Y. Ebina, M. Yamamoto, *Phys. Rev. B* **91**, 140410(R) (2015)
73. A. Rath, C. Sivakumar, C. Sun, S.J. Patel, J.S. Jeong, J. Feng, G. Stecklein, P.A. Crowell, C.J. Palmström, W.H. Butler, P.M. Voyles, *Phys. Rev. B* **97**, 045304 (2018)
74. P. Li, Y. Song, H. Dery, *Phys. Rev. B* **86**, 085202 (2012)
75. Y. Song, O. Chalaev, H. Dery, *Phys. Rev. Lett.* **113**, 167201 (2014)
76. Y. Fujita, M. Yamada, S. Yamada, T. Kanashima, K. Sawano, K. Hamaya, *Phys. Rev. B* **94**, 245302 (2016)
77. M. Yamada, Y. Fujita, M. Tsukahara, S. Yamada, K. Sawano, K. Hamaya, *Phys. Rev. B* **95**, 161304(R) (2017)
78. M. Yamada, T. Ueno, T. Naito, K. Sawano, K. Hamaya, *Phys. Rev. B* **104**, 115301 (2021)
79. Y. Fujita, M. Yamada, M. Tsukahara, T. Naito, S. Yamada, K. Sawano, K. Hamaya, *Phys. Rev. B* **100**, 024431 (2019)
80. M. Yamada, Y. Shiratsuchi, H. Kambe, K. Kudo, S. Yamada, K. Sawano, R. Nakatani, K. Hamaya, *J. Appl. Phys.* **129**, 183901 (2021)
81. K. Sawano, Y. Hoshi, S. Kubo, K. Arimoto, J. Yamanaka, K. Nakagawa, K. Hamaya, M. Miyao, Y. Shiraki, *Thin Solid Films* **613**, 24 (2016)
82. G. Schmidt, D. Ferrand, L.W. Molenkamp, A.T. Filip, B.J. van Wees, *Phys. Rev. B* **62**, R4790 (2000)
83. E.I. Rashba, *Phys. Rev. B* **62**, R16267 (2000)
84. A. Fert, H. Jaffrès, *Phys. Rev. B* **64**, 184420 (2001)
85. S. Takahashi, S. Maekawa, *Phys. Rev. B* **67**, 052409 (2003)
86. N. Tombros, C. Jozsa, M. Popinciuc, H.T. Jonkman, B.J. van Wees, *Nature* (London) **448**, 571 (2007)
87. T.-Y. Yang, J. Balakrishnan, F. Volmer, A. Avsar, M. Jaiswal, J. Samm, S.R. Ali, A. Pachoud, M. Zeng, M. Popinciuc, G. Güntherodt, B. Beschoten, B. Özyilmaz, *Phys. Rev. Lett.* **107**, 047206 (2011)
88. W. Han, R.K. Kawakami, *Phys. Rev. Lett.* **107**, 047207 (2011)
89. T. Suzuki, T. Sasaki, T. Oikawa, M. Shiraiishi, Y. Suzuki, K. Noguchi, *Appl. Phys. Express* **4**, 023003 (2011)
90. M. Ishikawa, T. Oka, Y. Fujita, H. Sugiyama, Y. Saito, K. Hamaya, *Phys. Rev. B* **95**, 115302 (2017)
91. A. Spiesser, H. Saito, Y. Fujita, S. Yamada, K. Hamaya, S. Yuasa, R. Jansen, *Phys. Rev. Appl.* **8**, 064023 (2017)
92. M. Yamada, M. Tsukahara, Y. Fujita, T. Naito, S. Yamada, K. Sawano, K. Hamaya, *Appl. Phys. Express* **10**, 093001 (2017)
93. T. Sasaki, T. Suzuki, Y. Ando, H. Koike, T. Oikawa, Y. Suzuki, M. Shiraiishi, *Appl. Phys. Lett.* **104**, 052404 (2014)
94. Y. Saito, T. Tanamoto, M. Ishikawa, H. Sugiyama, T. Inokuchi, K. Hamaya, N. Tezuka, *J. Appl. Phys.* **115**, 17C514 (2014)
95. S. Sato, R. Nakane, T. Hada, M. Tanaka, *Phys. Rev. B* **96**, 235204 (2017)
96. M. Ishikawa, M. Tsukahara, M. Yamada, Y. Saito, K. Hamaya, *IEEE Trans. Magn.* **54**, 1400604 (2018)
97. A. Fert, J.-M. George, H. Jaffrès, R. Mattana, *IEEE Trans. Electron Devices* **54**, 921 (2007)
98. H. Jaffrès, J.-M. George, A. Fert, *Phys. Rev. B* **82**, 140408(R) (2010)
99. P. Laczkowski, L. Vila, V.-D. Nguyen, A. Marty, J.-P. Attané, H. Jaffrès, J.-M. George, A. Fert, *Phys. Rev. B* **85**, 220404(R) (2012)
100. M. Tsukahara, M. Yamada, T. Naito, S. Yamada, K. Sawano, V.K. Lazarov, K. Hamaya, *Appl. Phys. Express* **12**, 033002 (2019)
101. M. Yamada, T. Naito, K. Sumi, K. Sawano, K. Hamaya, *IEEE Trans. Magn.* (forthcoming)
102. T. Naito, M. Yamada, S. Yamada, K. Sawano, K. Hamaya, *Phys. Rev. Appl.* **13**, 054025 (2020)
103. T. Naito, M. Yamada, Y. Wagatsuma, K. Sawano, K. Hamaya, *Phys. Rev. Appl.* (forthcoming) □



**Kohei Hamaya** has been a professor at Osaka University, Japan, since 2014, after working at The University of Tokyo and Kyushu University, Japan. He received his PhD degree in material science from the Tokyo Institute of Technology, Japan, in 2005. From 2005 to present, he has focused on semiconductor spintronics. Since 2008, Hamaya has explored low-temperature molecular beam epitaxy techniques on Heusler-compound films on semiconductors and oxides for spintronics devices. He is the director of the Center for Spintronics Research Network and Division of Spintronics Research Network, Osaka University, Japan. Hamaya can be reached by email at hamaya.kohei.es@osaka-u.ac.jp.



**Michihiro Yamada** is currently a specially appointed assistant professor at Osaka University, Japan. He received his PhD degree in materials science from Keio University, Japan, in 2016, focusing on the development of novel doping techniques in semiconductors. From 2016, he has studied spin injection and spin transport in Ge with Co-based Heusler contacts. His current research interests include Group-IV semiconductor spintronics devices with highly efficient spin injection from ferromagnetic Heusler/semiconductor heterojunctions. Yamada can be reached by email at michihiro@ee.es.osaka-u.ac.jp.